PROBABILITY CONCEPTS FOR GEO COLLISION RISK ASSESSMENT*

Alan B. Jenkin[(1)]

[(1)]*The Aerospace Corporation, El Segundo, CA 90245, USA, Email: Alan.B.Jenkin@aero.org*

ABSTRACT

This paper discusses probability concepts for computing short-term and long-term collision risk that account for correlation effects in geosynchronous orbit (GEO). The focus is on covariance-based methods, which have realistic computer resources requirements. For near-coplanar encounters, a collision probability formulation for position and velocity errors and general orbital motion was developed based on the theory of dynamical probability continua that has been used for debris cloud risk assessment. A method for assessing long-term risk with the purpose of selecting collision avoidance action thresholds on short-term risk is described. This methodology accounts for GEO-specific correlating effects and maintains consistency of uncertainty modeling between short- and long-term risk assessment.

1. INTRODUCTION

As the population of objects in geosynchronous orbit (GEO) has been growing, interest in quantitative assessment of collision risk posed to operational satellites has been increasing. Short-term risk assessment generally involves a predicted encounter between an operational satellite (the "primary") and another object (the "secondary"). Determination of the collision probability associated with the encounter can be used to support decisions regarding a collision avoidance action. Long-term collision risk assessment, i.e., collision probability over the duration of a mission, can be used to select action thresholds on encounter collision probability [1].

Geosynchronous orbits have unique correlational properties which must be accounted for in accurate collision probability assessment. These correlations are due to common orbital period and low inclination, as well as the dominant orbital perturbations. For non-operational satellites, longitude drifts slowly due to tesseral harmonics and SRP. Luni-solar gravity causes right ascension of ascending node (RAAN) and inclination to move together. SRP and luni-solar gravity cause eccentricity and argument of perigee to move together. Operational satellites actively control longitude and inclination via station keeping maneuvers. Risk assessment methods that do not account for these correlational effects may not yield accurate results for GEO. As an example, for a flux-based method to be accurate, it would require very high resolution, three-dimensional spatial and temporal binning of spatial density and velocity, and the binning would have to be implemented in the GEO rotating frame to retain longitude correlation. This paper discusses probability concepts for computing short-term and long-term collision risk that account for correlation effects in GEO.

2. GENERAL FORMULATION OF COLLISION PROBABILITY

A general formulation of collision probability involves a mapping M_{IO} between an input space of N-dimensional vectors $\underline{x}$ and an output space of 3-dimensional vectors $\underline{y}$. This mapping is illustrated in Fig. 1. An instance of the vector $\underline{y}$ is defined as the position vector at closest approach over a time interval [0,t]. The vector $\underline{x}$ consists of uncertain variables. These may include a position vector $\underline{r}$, velocity vector $\underline{v}$, solar radiation pressure coefficient, maneuver times and ΔVs, classical orbital elements, etc. In the output space there is a region Y_C of closest approach vectors that result in a collision. In the input space there is a region X_C that maps to Y_C. The probability of collision is then obtained by integrating the probability density function (PDF) of $\underline{x}$, $f_{\underline{x}}(\underline{x})$, over X_C.

$$p_C = \int_{X_C} f_{\underline{x}}(\underline{x})\, dV_{\underline{x}} \qquad (1)$$

The variables in vector $\underline{x}$ are selected to be uncorrelated. The mapping M_{IO} between the input space and output space will include all correlational properties. (For a primer on the theory of uncertain variables and PDFs, see [2]). The most direct way to implement this general formulation is via Monte Carlo analysis. For each Monte Carlo iteration, each member

Proc. '5th European Conference on Space Debris', Darmstadt, Germany 30 March – 2 April 2009, (ESA SP-672, July 2009)

of $\underline{x}$ is randomly sampled according to its PDF. A precision trajectory is then generated using a high-fidelity propagator, and a close approach analysis is performed to obtain the position vector $\underline{y}$ at closest approach over the time interval [0,t] (the global closest approach over the time interval, not a local close approach). If the resulting value of $\underline{y}$ is contained in Y_C, then a collision counter is incremented. After all the iterations are finished, the collision probability is computed by dividing the collision counter by the total number of Monte Carlo iterations. The advantage of this method is that it is relatively simple to formulate and implement. It also places minimal restrictions on the selection of uncertain variables in $\underline{x}$. The disadvantage of this method is that the resolution of collision probability value is limited by computer resources (memory and speed). For example, in order to be able to resolve a collision probability value of 10^{-6}, at least 10^7 to 10^9 Monte Carlo iterations will be needed. The rest of this paper will focus on more specialized methods that use covariance for assessing collision probability, since these methods have more realistic computer resource requirements.

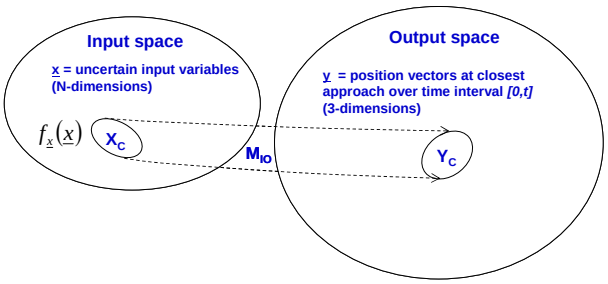

Figure 1. Mapping from input space of uncertain, uncorrelated variables to closest approach vectors.

3. COVARIANCE-BASED PROBABILITY OF COLLISION

Covariance-based methods for determining collision probability during an encounter assume a position error PDF that is Gaussian. For example, the position PDF for the secondary satellite, $f_{\underline{r}}(\underline{r})$ is

$$f_{\underline{r}}(\underline{r}) = G(\underline{r}, \underline{r}_N, C_{rr}) = \frac{1}{(2\pi)^{3/2}\left|\det C_{rr}\right|^{1/2}} e^{-\frac{1}{2}(\underline{r}-\underline{r}_N)^T C_{rr}^{-1}(\underline{r}-\underline{r}_N)} \quad (2)$$

where G denotes a Gaussian PDF with mean $\underline{r}_N$ (the nominal predicted position) and covariance C_{rr} (the position error covariance). The covariance can be computed via any of several methods. One way is to propagate the covariance at the orbit determination epoch to the current time via the state transition matrix $\Phi(\underline{r}_{0_N}, \underline{v}_{0_N}, t)$, which maps perturbations in the initial state vector $\underline{x}_0 = [\underline{r}_0 \quad \underline{v}_0]$ to the current state vector $\underline{x} = [\underline{r} \quad \underline{v}]$, and is well documented in the astrodynamics literature.

$$C_x(t) = \begin{bmatrix} C_{rr} & C_{rv} \\ C_{vr} & C_{vv} \end{bmatrix} = \Phi(\underline{r}_{0_N}, \underline{v}_{0_N}, t) C_{x_0} \Phi^T(\underline{r}_{0_N}, \underline{v}_{0_N}, t) \quad (3)$$

where $\underline{r}_{0_N}$ and $\underline{v}_{0_N}$ are the nominal position and velocity at orbit determination epoch. The size of the covariance can be understood in terms of its 3-sigma error ellipsoid, the surface of which is described by the equation

$$\frac{1}{2}(\underline{r}-\underline{r}_N)^T C_{rr}^{-1}(\underline{r}-\underline{r}_N) = \frac{9}{2} \quad (4)$$

A high value of collision probability (e.g., > 0.001) means the miss distance will be low and the error covariance ellipsoid is small. A low collision probability value (e.g., < 10^{-6}) can mean one or both of two possibilities. If the error covariance ellipsoid is small, then the miss distance will be high. If the error covariance ellipsoid is large, then a low probability value means the position knowledge is poor. In the latter case, the actual risk will be low only if the covariance at that encounter is accurate, i.e., not conservatively large. In other words, the position could truly be anywhere within the covariance region in accordance with the Gaussian probability density function (PDF). The true collision risk could be higher than indicated by the probability value if the predicted miss distance is low and the covariance is conservatively large. This may be an issue for models of covariance that only contain the secular variation with time and do not include the periodic variation.

Another important consideration is that low collision probabilities at many encounters with large covariances can sum to a large collision probability over mission timeframe and constellation members. Therefore, repeated occurrences of low collision probabilities should not be interpreted as an indication of low overall collision risk.

4. SHORT-TERM RISK ASSESSMENT

GEO encounters can generally be classified as either non-coplanar encounters or near-coplanar encounters. (This discussion does not include secondary objects in non-synchronous orbits or GEO-transiting orbits). A non-coplanar encounter will occur if either satellite has drifting inclination and RAAN. Encounter velocities can range up to 1.7 km/s. The cross-track component of velocity dominates over the other two components.

Encounter time is short. The majority of encounters experienced by a GEO satellite over its mission time frame will be non-coplanar. A near-coplanar encounter will most likely occur when both satellites are in orbits with near-zero inclination. In this case the encounter velocity will generally be low (on the order of 1 m/s). All three velocity components may be commensurate. The encounter time may be extended.

For non-coplanar encounters, the motion between the primary and secondary can be modeled as rectilinear, and the position error covariance during the encounter can be modeled as static. There are several formulations in the literature that handle the static Gaussian/rectilinear motion case [3-6]. These methods effectively involve projecting the position error Gaussian PDF into the encounter plane, which is orthogonal to the relative velocity between the primary and secondary. The collision probability is then determined by integrating the PDF over the satellite collision cross-section A_C in the encounter plane. These formulations are very computationally efficient.

The static Gaussian/rectilinear formulation may be applicable to a near-coplanar encounter if the covariance is small compared to the relative range of motion between the two satellites. This may be the case when both orbits can be produced by a high-accuracy orbit determination method. Otherwise, the relative motion will not be rectilinear, and the covariance will not be static. If the covariance is large, many cycles of the relative trajectory may remain in the general region of the covariance error ellipsoid. In addition, the propagated position error PDF will no longer be Gaussian if enough time passes for it to spread around part of the orbit arc. A formulation is presented here that can be applied to non-coplanar encounters with improved generality. The formulation is based on the theory of dynamical probability continua that has been used to assess risk posed by debris clouds formed by breakups [7]. This is motivated by the fact that a position error PDF will follow the same orbital motion as a debris cloud. The development will start with the case in which there are only initial velocity errors, since this follows the formulation for debris clouds. Then the formulation will be expanded to include initial position errors.

The formulation starts with a mapping from an initial velocity space at orbit determination epoch to position space at a current time t. This mapping is illustrated in Fig. 2 and is represented by the propagator function

$$\underline{r}_s(t) = P_r(\underline{v}_{s0}, t) \tag{5}$$

In the figure, P denotes the primary and S denotes the secondary. The initial velocity errors are assumed to apply to the secondary. For Gaussian velocity errors, the initial velocity PDFs for both primary and secondary can be represented by one initial velocity PDF with covariance equal to the sum of the velocity covariances of the two satellites. The mapping between initial velocity space and current position space will be bijective (one-to-one) as long as the current position PDF has not wrapped around the Earth and overlapped upon itself. Therefore, as the primary satellite traces a path in current position space, it will trace an equivalent path in initial velocity space. The advantage of considering the primary path in initial velocity space is that the PDF in that space is time invariant. The primary will have a time-varying collision cross-section $A_{C\underline{v}0}$ that will sweep out a volume $V_{\underline{v}0}$ over a time interval [0,t]. The collision probability is then obtained by integrating the PDF $f_{\underline{v}_{s0}}(\underline{v}_{s_0})$ over $V_{\underline{v}0}$.

$$p_C = \int_{V_{\underline{v}_0}} f_{\underline{v}_{s0}}(\underline{v}_{s_0})\, dV_{\underline{v}_0} = \int_{\substack{\text{Primary path} \\ \text{swept during [0,t]}}} \int_{A_{C_{v_0}}} f_{\underline{v}_{s0}}(\underline{v}_{s_0})\, dA_{C_{v_0}}\, dv_{s_0} \tag{6}$$

The integral has been formulated to include integration over the collision cross-section $A_{C\underline{v}0}$ in the case the PDF varies over the collision cross-section, which would occur if the satellite is large and the orbit determination is highly accurate.

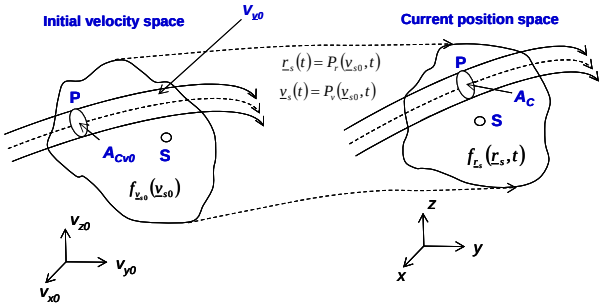

Figure 2. Mapping from initial velocity space to current position space.

To make the integral implementable, it is necessary to relate displacements in initial velocity space to displacements in current position space. This can be accomplished by considering differential increments in position and cross-sectional area, which are illustrated in Fig. 3.

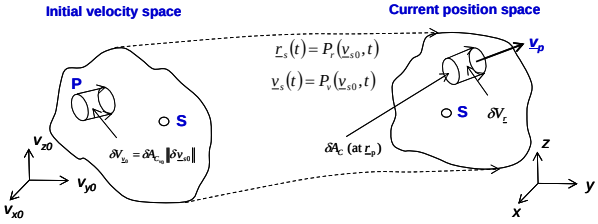

Figure 3. Differential increments in initial velocity space and current position space.

The first step is to obtain the first variation of the position of the secondary due to perturbations in the initial velocity and time. This can be obtained by differentiating the propagator function that maps initial velocity space to current position space.

$$\delta \underline{r}_s = \frac{\partial P_r}{\partial \underline{v}_{s_0}} \delta \underline{v}_{s_0} + \frac{\partial P_r}{\partial t} \delta t \tag{7}$$

The velocity partial derivative is the velocity to position component of the state transition matrix.

$$\frac{\partial P_r}{\partial \underline{v}_{s_0}} = \Phi_{rv}\left(v_{s_0}, t\right) \tag{8}$$

The time partial derivative is simply the velocity of the secondary if it has an initial velocity $\underline{v}_{S0}$.

$$\frac{\partial P_r}{\partial t} = \frac{\partial \underline{r}_s}{\partial t} = \underline{v}_s \tag{9}$$

where $\underline{v}_s$ is computed by the propagator function from initial velocity space to current velocity space.

$$\underline{v}_s = P_{\underline{v}}\left(\underline{v}_{s_0}, t\right) \tag{10}$$

The constraint that relates the two spaces is that the positional displacement of the secondary matches the displacement of the primary.

$$\begin{aligned} &\underline{v}_p \delta t = \delta \underline{r}_p \\ &\equiv \delta \underline{r}_s = \Phi_{rv}\left(v_{s_0}, t\right) \delta \underline{v}_{s_0} + \underline{v}_s \delta t \end{aligned} \tag{11}$$

This can be rearranged as follows.

$$\begin{aligned} \Phi_{rv}\left(v_{s_0}, t\right) \delta \underline{v}_{s_0} &= \left(\underline{v}_p - \underline{v}_s\right) \delta t \\ &= \underline{v}_{ps} \delta t \end{aligned} \tag{12}$$

Due to the constraint in Eq. 11, $\underline{v}_s$ is now the velocity of the secondary <u>if it is at the same location as the primary at time t</u>. Note that $\underline{v}_s$ is <u>not</u> in general the nominal predicted velocity of the secondary. This formulation will therefore account for the fact that the position error field moves relative to the nominal predicted position of the secondary. This is analogous to the motion of fragments in a debris cloud relative to the debris cloud center.

Differential volumes swept out by displacements in initial velocity and current position space are needed to reformulate the integration of Eq. 6 in current position space. They can be formulated as follows.

$$\delta V_{\underline{v}_0} = \delta A_{C_{v_0}} \left\| \delta \underline{v}_{s0} \right\| \tag{13}$$

$$\delta V_{\underline{r}} = \delta A_C \left\| \delta \underline{r}_{ps} \right\| = \delta A_C \left\| \underline{v}_{ps} \delta t \right\| \tag{14}$$

From advanced calculus, Eqs. 12-14 can be combined to relate the differential volumes via the Jacobian of the mapping from initial velocity to current position space.

$$\delta V_{\underline{r}} = \left| J \right| \delta V_{\underline{v}_{s_0}} \tag{15}$$

where

$$J = \det \Phi_{rv}\left(\underline{v}_{s_0}, t\right) \tag{16}$$

Solving Eq. 15 for $\delta V_{\underline{v}_{s_0}}$ and substituting in Eqs. 13 and 14 yields

$$\delta A_{C_{v_0}} \left\| \delta \underline{v}_{s0} \right\| = \frac{1}{\left| J \right|} \delta A_C \left\| \underline{v}_{ps} \right\| \delta t \tag{17}$$

By substituting Eq. 17 into Eq. 6, the integral can now be expressed in current position space.

$$p_C = \int_{\substack{\text{Primary path} \\ \text{swept during [0,t]}}} \int_{\substack{\text{Satellite} \\ \text{positions } \underline{r}_p \\ \text{in } A_C}} f_{\underline{v}_{s0}}\left(\underline{v}_{s_0}(\tau)\right) \frac{1}{\left| J\left(\underline{v}_{s_0}(\tau), \tau\right) \right|} \left\| \underline{v}_p(\tau) - \underline{v}_s\left(\underline{v}_{s_0}(\tau), \tau\right) \right\| dA_C d\tau \tag{18}$$

where $\underline{v}_s$ is obtained from Eq. 10. To evaluate the integral, it is necessary to solve for $\underline{v}_{s0}$ from $\underline{r}_p$. This is accomplished by inverting the propagator function.

$$\underline{v}_{s0} = P_{\underline{r}}^{-1}\left(\underline{r}_p(t), t\right) \tag{19}$$

This must be done numerically via differential correction. If the integrand in Eq. 18 does not vary significantly across the collision cross-section A_C, (i.e., satellite is not large relative to the position error covariance), the area integral can be removed.

$$p_C = \int_{\substack{\text{Primary path} \\ \text{swept during [0,t]}}} f_{\underline{v}_{s0}}\left(\underline{v}_{s_0}(\tau)\right) \frac{1}{\left| J\left(\underline{v}_{s_0}(\tau), \tau\right) \right|} \left\| \underline{v}_p(\tau) - \underline{v}_s\left(\underline{v}_{s_0}(\tau), \tau\right) \right\| A_C d\tau \tag{20}$$

The formulation can now be expanded to include initial position errors by treating the velocity error formulation as a conditional probability with condition that the initial position is fixed at $\underline{r}_0$. The total collision probability is then obtained by integrating over the position error PDF $f_{\underline{r}_{s0}}\left(\underline{r}_{s_0}\right)$.

$$p_C = \int_{\substack{r_0 \\ \text{PDF}}} p_{C_{\underline{r}_0}}\left(\underline{r}_0\right) f_{\underline{r}_{s0}}\left(\underline{r}_{s_0}\right) dV_{\underline{r}_0} \tag{21}$$

Equations 20 and 21 can be combined to yield an expression in terms of the joint initial position-velocity PDF. The dependence of other quantities in the integrand on $\underline{r}_0$ is explicitly shown.

$$p_C = \int_{\substack{r_0 \\ \text{PDF}}} \int_{\substack{\text{Primary path} \\ \text{swept during [0,t]}}} \int_{\substack{\text{Satellite} \\ \text{positions} \\ \text{in } A_C}} f_{\underline{r}_{s_0},\underline{v}_{s_0}}\left(\underline{r}_{s_0},\underline{v}_{s_0}\left(\underline{r}_{s_0},\tau\right)\right)\frac{1}{\left|J\left(\underline{r}_{s_0},\underline{v}_{s_0}\left(\underline{r}_{s_0},\tau\right),\tau\right)\right|} \left\|\underline{v}_p(\tau)-\underline{v}_s\left(\underline{r}_{s_0},\underline{v}_{s_0}\left(\underline{r}_{s_0},\tau\right),\tau\right)\right\| dA_C\, d\tau\, dV_{\underline{r}_0} \quad (22)$$

where

$$\underline{v}_{s0} = P_{\underline{r}}^{-1}\left(\underline{r}_p(t),\underline{r}_{s0},t\right) \quad (23)$$

$$J = \det \Phi_{rv}\left(\underline{r}_{s_0},\underline{v}_{s_0},t\right) \quad (24)$$

$$\underline{v}_s = P_{\underline{v}}\left(\underline{r}_{s_0},\underline{v}_{s_0}\left(\underline{r}_{s_0},t\right),t\right) \quad (25)$$

If the integrand in Eq. 22 does not vary significantly across the collision cross-section A_C, the area integral can be removed.

$$p_C = \int_{\substack{r_0 \\ \text{PDF}}} \int_{\substack{\text{Primary path} \\ \text{swept during [0,t]}}} f_{\underline{r}_{s_0},\underline{v}_{s_0}}\left(\underline{r}_{s_0},\underline{v}_{s_0}\left(\underline{r}_{s_0},\tau\right)\right)\frac{1}{\left|J\left(\underline{r}_{s_0},\underline{v}_{s_0}\left(\underline{r}_{s_0},\tau\right),\tau\right)\right|} \left\|\underline{v}_p(\tau)-\underline{v}_s\left(\underline{r}_{s_0},\underline{v}_{s_0}\left(\underline{r}_{s_0},\tau\right),\tau\right)\right\| A_C\, d\tau\, dV_{\underline{r}_0} \quad (26)$$

Equation 26 involves numerical evaluation of a four-dimensional integral. Implementation is still feasible (in comparison to a direct Monte Carlo method), but the run time will be much higher than for the static Gaussian/rectilinear formulation. Ideally, covariances should be small enough (due to accurate orbit determination) so that only a small fraction of encounters require this method.

This formulation is applicable for general initial position and velocity PDFs. However, for GEO encounters, the PDF will be Gaussian and contain the combined errors from the primary and secondary.

$$f_{\underline{r}_{s_0},\underline{v}_{s_0}}\left(\underline{r}_{s_0},\underline{v}_{s_0}\right) = G\left(\underline{x}_{s_0},\underline{x}_{s_{0N}},C_{x_0}\right) = \frac{1}{(2\pi)^{3/2}\left|\det C_{x_0}\right|^{1/2}} e^{-\frac{1}{2}\left(\underline{x}_{s_0}-\underline{x}_{s_{0N}}\right)^T C_{v0}^{-1}\left(\underline{x}_{s_0}-\underline{x}_{s_{0N}}\right)} \quad (27)$$

where the combined covariance is the sum of the covariances of the primary and secondary.

$$C_{x_0} = C_{x_0 p} + C_{x_0 s} \quad (28)$$

The formulation represented by Eqs. 23-25 and 22 or 26 has several advantages. It applies to general orbital motion and is not restricted to rectilinear or linear motion. As a result, the method can be used to compute collision probability over longer periods of time (weeks to months) as the position error field spreads out along the orbit arc around the Earth. However, it may be advisable to augment the formulation with SRP coefficient as an uncertain variable, since recent results by Chao [8] show that SRP coefficient uncertainty has a significant effect on GEO propagation error. A caveat on the method is that the integration in current position space is only equivalent to integration in initial velocity space as long as the path of the primary in initial velocity space does not significantly retrace itself. If retracing occurs, the integration in current position space will overbook the accumulation of probability in initial velocity space, so the consequence will be an overestimate (conservative). However, the effect of retracing is expected to be limited by secular growth of the position error covariance ellipsoid, which is caused by the component of the initial velocity error covariance in the orbit-tangential direction.

5. NUMERICAL EXAMPLE OF A NEAR-COPLANAR ENCOUNTER

A hypothetical example of a near-coplanar encounter was generated in order to partially demonstrate the method. The initial orbital elements at common epoch are shown in Table 1. Figure 4 shows the range between the primary and secondary over the 10-day forecast period.

Table 1. Initial orbital elements at common epoch for a hypothetical near-coplanar GEO encounter.

Satellite	*a*	*e*	*i*	*Ω*	*ϖ*	*M*
	km		deg	deg	deg	deg
Primary	42165.5	0.002	0.0242	83.889646	89.865869	265.135957
Secondary	42165.9	0.002	0.0270	83.899620	99.865874	255.158225

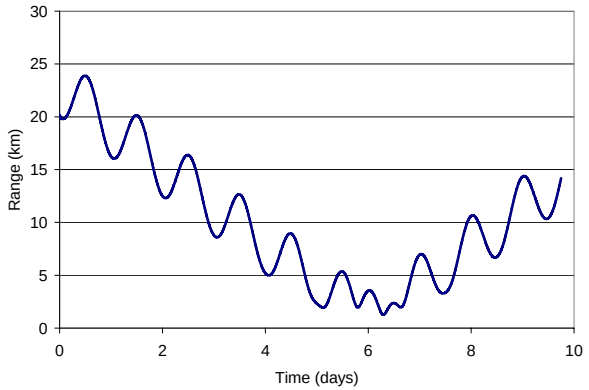

Figure 4. Range between primary and secondary over 10-day forecast.

A version of program DEBRIS [7] modified with a Gaussian velocity error PDF in place of a fragment velocity distribution was used to generate a 10-day forecast of collision probability. This code effectively evaluates Eqs. 19, 10 and 20. The propagator functions (Eqs. 5 and 10) model Keplerian + secular J_2 motion. While this is acceptable for the purpose of demonstrating the method, for real-world applications luni-solar gravity, SRP, and tesseral harmonics should be included. A collision radius of 10 m was selected, which yields a circular cross-sectional area A_C of 314 m^2. Only initial velocity errors were modeled because development of a version of DEBRIS with initial position errors is still in progress. The run took 11.13 CPU seconds on one processor of an UltraSPARC 3i.

The initial velocity error covariance was determined to least-squares best fit a secular model of position errors versus. time that was used in the study by Jenkin and Peterson [1]. This secular model is a fit to TLE data residuals and is an average over GEO objects The model gives three-sigma position errors (km) in the TNW frame (T = tangential, N = in-plane normal to tangential, W = cross-track) versus time t (days).

$$\begin{aligned} 3\sigma_T &= 28.08 + 2.16t + 0.03t^2 \\ 3\sigma_N &= 17.94 + 0.21t \\ 3\sigma_W &= 7.59 + 0.45t \end{aligned} \qquad (29)$$

The Clohessy-Wiltshire transition matrix formulation was used to map the initial velocity error covariance to position error covariance at current time.

$$C_{rr}(t) = \Phi_{rv}\left(\underline{\nu}_{s_{0N}}, t\right) C_{vv_0} \Phi_{rv}{}^{T}\left(\underline{\nu}_{s_{0N}}, t\right) \qquad (30)$$

The resulting three-sigma TNW position errors, which contain secular and periodic components, were extracted and differenced with the secular model values to form the residuals that are minimized in the determination of the velocity error covariance. The resulting initial velocity error covariance, expressed in the TNW frame in units of $(km/s)^2$, is

$$C_{vv_0)TNW} = \begin{bmatrix} 7.922068\text{E-}11 & 1.640428\text{E-}09 & 0 \\ 1.640428\text{E-}09 & 1.089637\text{E-}07 & 0 \\ 0 & 0 & 9.118412\text{E-}08 \end{bmatrix} \qquad (31)$$

Figures 5-7 show the three-sigma TNW position errors from both the secular model and the velocity error covariance model (Eq. 30). It can be seen that, for the T component, the secular trend in the velocity error covariance model fits the secular model relatively well except toward the end of the 10-day interval. The fit is not as good in the W component, and especially not in the N component. Increasing the N-component of the velocity error covariance to improve the N component fit introduces a very large amplitude in the periodic portion of the T component. Therefore, the velocity error covariance by itself is not sufficient. The position error covariance is needed to improve the N component fit and should be included in real-world applications via Eq. 22 or 26.

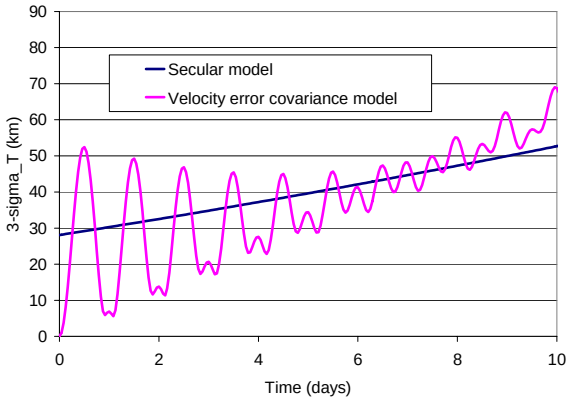

Figure 5. Three-sigma T-component of position error.

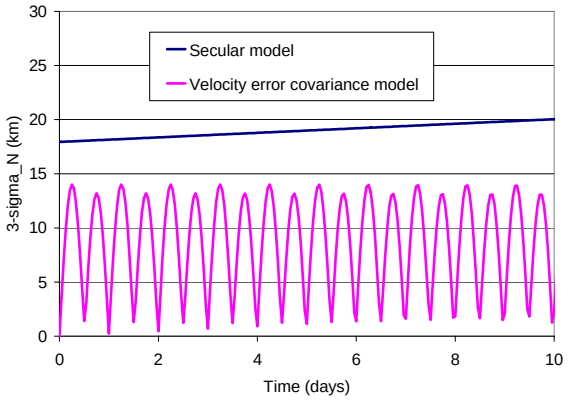

Figure 6. Three-sigma N-component of position error.

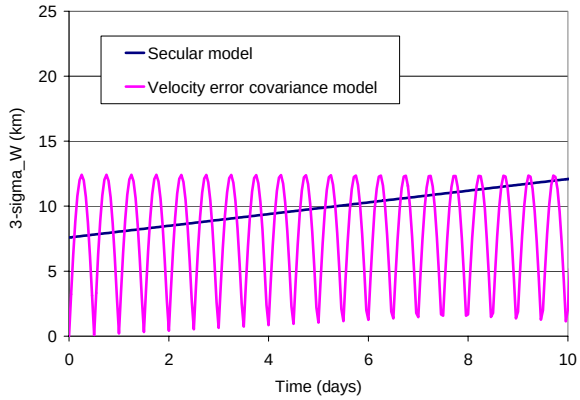

Figure 7. Three-sigma W-component of position error.

Figures 8-11 show results from the DEBRIS run. Figure 8 shows the path of the primary satellite in initial velocity error space while it is inside the six-sigma error ellipsoid. Figure 9 shows the probability accumulation rate versus time over the 10-day interval.

It is seen that the peaks are interrupted by gaps where the probability rate drops to zero. To see this in more detail, Fig. 10 shows a window of the same plot from 3.75 to 4.75 days. This effect is caused by contraction of the position error covariance N and W components due to periodic variation (see Figs. 6 and 7). As these covariance components contract, the primary at first experiences an increase in probability density, but then experiences a decrease as the three-sigma error ellipsoid is drawn in to the secondary nominal position. Figure 11 shows the cumulative collision probability versus time. It is seen that the total encounter probability accumulates continuously across the 10-day forecast period. Attempting to compute collision probability at only the conjunctions (local minima in range) would not yield an accurate result.

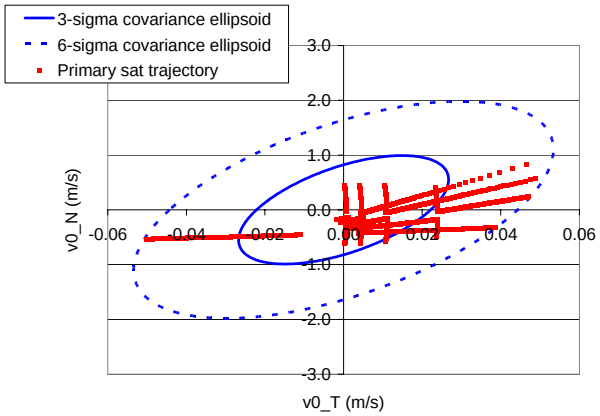

Figure 8. Path of the primary in initial velocity space.

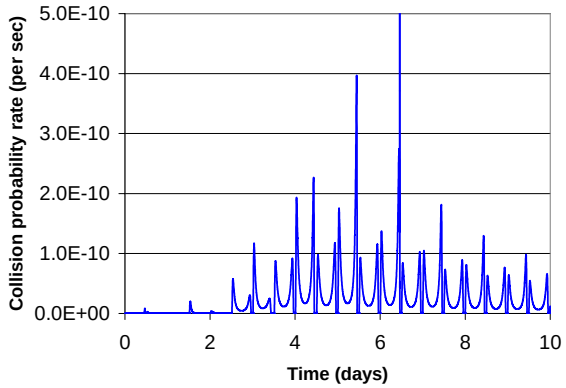

Figure 9. Collision probability accumulation rate versus time over the 10-day forecast period.

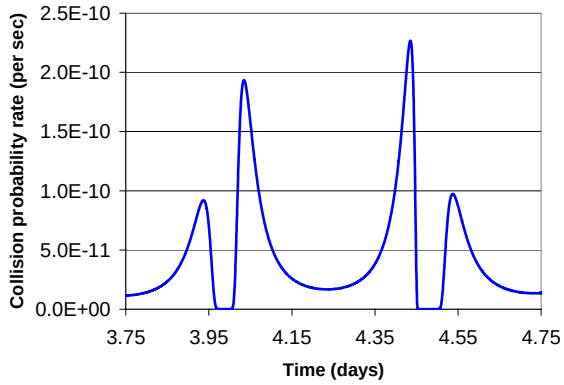

Figure 10. Collision probability accumulation rate versus time over the time interval from 3.75 to 4.75 days.

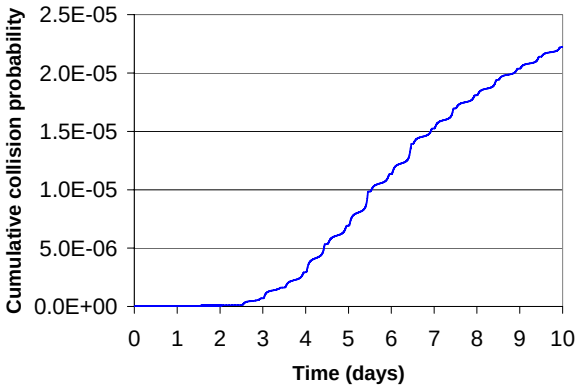

Figure 11. Cumulative collision probability versus time.

6. LONG-TERM RISK ASSESSMENT

Determination of the long-term collision risk over mission life can be used to select an action threshold on encounter collision probability [1]. For this purpose, the long-term risk assessment should be based on uncertainty modeling that is consistent with the short-term risk assessment. Therefore, statistically representative position and velocity error covariances should play a role in long-term collision probability determination. Additional uncertainties that play a role are future population growth, repeated station keeping maneuvers by operational satellites, and satellite failures. One way to model these latter uncertainties is by using historical data from recent years to represent future trends during the next few years. This is an indirect, data-driven method that does not explicitly model uncertain, uncorrelated input variables.

The following method for assessing long-term collision risk accounts for both classes of uncertainties. It is an extension of the method used in [1]. A historical

database of orbit determination products is established that contains state vectors (e.g., TLEs) and corresponding position and velocity error covariances. A conjunction simulation tool (e.g., Collision Vision [1]) is used with the database to determine conjunctions over a long time interval (e.g., one year). During the conjunction simulation, the state vectors and covariances are propagated over a short time interval (e.g., 10 days) and then refreshed from the database to account for maneuvers, rectify propagation errors, etc. The covariance propagation should include periodic variation and not only secular variation to prevent underestimating risk. The refresh time interval should be the same as the forecast interval over which the action threshold will be applied so that the position error covariance growth will be accurately represented. For each resulting non-coplanar conjunction, the encounter collision probability is computed using the static Gaussian/rectilinear motion formulation. Clusters of near-coplanar conjunctions are grouped into near-coplanar encounters, and the position and velocity error/general motion formulation is used to compute collision probability. The resulting collision probabilities from all encounters are then combined. Direct summation of the collision probabilities will be accurate if the sum is small (e.g., < 0.1). Otherwise, they should be combined via the formulation for general independent events.

$$p_{C_{Total}} = 1 - \prod_{i=1}^{N} \left(1 - p_{C_i}\right) \qquad (32)$$

7. CONCLUSIONS

This paper presented probability concepts for computing short-term and long-term collision risk that account for correlation effects in GEO. The focus was on covariance-based methods, which are less demanding on computer resources than a direct Monte Carlo approach. For computing short-term collision probability, the static Gaussian/rectilinear motion formulation can be used to compute collision probability for non-coplanar encounters. Periodic variation of covariance should be included to prevent underprediction of risk when predicted miss distance is low. For near-coplanar encounters, a collision probability formulation for position and velocity errors and general orbital motion was developed based on the theory of dynamical probability continua that has been used for debris cloud risk assessment. This formulation can be used to predict out for longer periods (weeks to months) as the position error field spreads around GEO. Long-term collision probability can be used to select action thresholds on short-term probability. Long-term collision probability can be determined by using a conjunction simulation with a database of historical state vectors and covariances, along with the short-term risk methods, to generate a statistically representative set of encounter collision probabilities. This methodology accounts for GEO-specific correlating effects and maintains consistency of uncertainty modeling between short and long-term risk assessment.

8. ACKNOWLEDGMENTS

This work reflects research conducted under U.S. Air Force Space and Missile Systems Center Contract FA8802-09-C-0001. The authors wish to thank several individuals for their support of this work and assistance in preparing this paper. Technical committee members M.E. Sorge, E.T. Campbell, and W.S. Campbell provided technical review of the paper. C.P. Griffice and M.E. Vojtek provided internal programmatic support for this work. The Aerospace Corporation's Office of Technical Relations and Vince Caponpon of the Department of the Air Force, SMC/EAFV, provided publication clearance review.

9. REFERENCES

1. Jenkin, A.B., Peterson, G.E., "Collision Risk Management in Geosynchronous Orbit," Advances in Space Research, Vol. 34, Issue 5, 2004, pp 1188-1192.
2. Papoulis, A., *Probability, Random Variables, and Stochastic Processes*, McGraw-Hill, New York, 1965.
3. Foster, J.L., Estes, H.S., "A Parametric Analysis of Orbital Debris Collision Probability and Maneuver Rate for Space Vehicles," NASA JSC 25898, August 1992.
4. Khutorovsky, Z.N., Boikov, V.F., Kamensky, S.Y., "Direct Method for the Analysis of Collision Probability of Artificial Space Objects in LEO: Techniques, Results, and Applications," Proceedings of the First European Conference on Space Debris, ESA SD-01, pp. 491-508, 1993.
5. Chan, F.K., *Spacecraft Collision Probability*, Chapter 5, The Aerospace Press, El Segundo, California, 2008.
6. Patera, R.P., "General Method for Calculating Satellite Collision Probability," Journal of Guidance, Control, and Dynamics, Vol. 24, No.4, July-August 2001, pp. 716-722.
7. Jenkin, A.B., "Probability of Collision During the Early Evolution of Debris Clouds," Acta Astronautica, Vol. 38, Nos 4-8, pp. 525-538, 1996.
8. Chao, C.C., Campbell, W.S., "Estimating Solar Radiation Pressure for GEO Debris," Fifth European Conference on Space Debris, March 30-April 2, 2009.